

# Structure and properties of high damping Fe-Ga based alloys

I. S. Golovin<sup>1\*</sup>, V. V. Palacheva<sup>1</sup>, A. A. Emdadi<sup>1</sup>, M. Yu. Zadorozhnyy<sup>1</sup>, A. I. Bazlov<sup>1</sup>,  
M. V. Gorshenkov<sup>1</sup>, A. V. Pozdniakov<sup>1</sup>, E. S. Savchenko<sup>1</sup>, J. Cifre<sup>2</sup>, R. Barbin<sup>3</sup>, J. Zhu<sup>4</sup>,  
S. A. Golovin<sup>4</sup>

<sup>1</sup>National University of Science and Technology “MISIS”, Leninsky ave. 4, 119049 Moscow, Russia

<sup>2</sup>Universitat de les Illes Balears, Ctra. de Valldemossa, km.7.5, E-07122 Palma de Mallorca, Spain

<sup>3</sup>ACOEM, Metrovib, 200, Chemin des Ormeaux, F-69578 Limonest Cedex, France

<sup>4</sup>University of Science and Technology Beijing, Beijing 100083, P. R. China

<sup>5</sup>Tula State University, Lenin ave. 84, 300012 Tula, Russia

## Abstract

Fe-Ga and Fe-Ga-Al alloys are studied by different mechanical spectroscopy techniques, conventional microscopy, DSC and dilatometry. Main contribution to amplitude dependent damping is assigned to magnetomechanical damping, which is very sensitive to structural state of alloys. Both temperature dependent thermally activated relaxation effects and effects due to phase transitions are discussed in terms of alloy structures and their ordering.

Key words: Fe-Ga, internal friction, damping, ordering

## 1. Introduction

The Fe-Ga alloys have recently become the focus of attention due to their giant magnetostriction in low saturation magnetic fields and good mechanical properties, except maybe low ductility. The magnetostriction ( $\lambda$ ) of single Fe-Ga crystals approaches 400 ppm along the  $\langle 100 \rangle$  direction [1]. The magnetostriction of polycrystalline Fe-Ga exhibits a peak near 19 % of 270 ppm [2]. Galfenols have the potential to be widely used in magnetostrictive actuators and sensor devices. They are also good candidates for damping applications [3]. According to the Smith and Birchak's theory [4], the maximal value of damping is proportional to  $\lambda$  of ferromagnetic materials:  $Q_{\max}^{-1} \sim \lambda$ .

It is believed that an increase in the magnetostriction of Fe-Ga alloys is due to the preferential  $\langle 001 \rangle$  Ga-Ga pairing in the disordered body centered cubic (bcc) structure [5]. Fe-Ga alloys are known by ordering of Ga atoms in bcc iron: the type of order depends on temperature and % Ga atoms (Fig. 1 [6]). Ordering decreases mobility of magnetic domain walls (MDW) and dislocations, leads to low ductility and decreases damping capacity (DC).

The formation of the equilibrium fcc L1<sub>2</sub> ordered phase below 630 °C according to the *equilibrium* Fe-Ga diagram (Fig. 1a) is rather slow, and in most cases the

ordering develops in accordance with the *metastable* diagram (Fig. 1b); at room temperature it is presented by a mixture of A2 and D0<sub>3</sub> phases. Quenching suppresses the formation of the D0<sub>3</sub> structure in favor of a disordered A2 structure and creates freeze-in vacancies. Furnace cooling or annealing of quenched samples may produce two-phase mixture of A2 + D0<sub>3</sub> (or L1<sub>2</sub>) for alloys with 11–20 % Ga.

Taking into account that the Fe-Ga metastable diagram is similar to the Fe-Al phase diagram, it is not surprising that alloys of both systems have a lot in common. Both Al and Ga enhance the magnetostriction of bcc Fe, making a magnetoelastic contribution to damping capacity. Atomic ordering in both systems (equilibrium long-range D0<sub>3</sub> in Fe-Al and equilibrium L1<sub>2</sub> in Fe-Ga) is expected to decrease damping due to pinning of MDW at antiphase boundaries. A short range D0<sub>3</sub> ordering may take place in both systems under certain conditions: e.g. at slow cooling or annealing.

## 2. Experimental procedure

### 2.1. Samples

In this paper we use at.%. The Fe-Ga and Fe-Ga-

\*Corresponding author: e-mail address: [i.golovin@isis.ru](mailto:i.golovin@isis.ru)

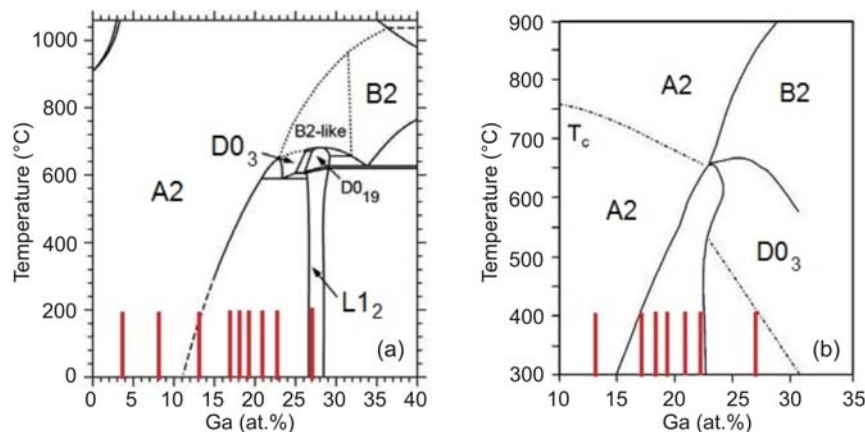


Fig. 1. Stable (a) and metastable (b) Fe-Ga phase diagrams adopted from Ref. [6]. Vertical lines indicate compositions of studied binary alloys.

Table 1. Studied alloys

<i>n</i>	Nominal composition	Structure according to E.D/non-E.D
01	Fe-3Ga	A2
02	Fe-8Ga	A2
03	Fe-13Ga	A2 + L1 <sub>2</sub> /D0 <sub>3</sub>
04	Fe-17Ga (NbC)*	A2 + L1 <sub>2</sub> /D0 <sub>3</sub>
05	Fe-18Ga (C, B)	A2 + L1 <sub>2</sub> / D0 <sub>3</sub>
06	Fe-19Ga	A2 + L1 <sub>2</sub> /D0 <sub>3</sub>
07	Fe-21Ga*	A2 + L1 <sub>2</sub> /D0 <sub>3</sub>
08	Fe-22Ga	A2 + L1 <sub>2</sub> /D0 <sub>3</sub>
09	Fe-27Ga	L1 <sub>2</sub> /D0 <sub>3</sub>
10	Fe-8Ga-4Al	unknown
11	Fe-13Ga-5Al	unknown
12	Fe-12Ga-6Al	unknown
13	Fe-9Ga-8Al	unknown
14	Fe-6Ga-12Al	unknown
15	Fe-18Ga-5Al	unknown

ED and n-ED – equilibrium and non-equilibrium phase diagrams

\* – forging plus rolling

-Al alloys were produced by direct solidification. Most of the samples were annealed at 1000 °C for 40 min, then (i) water quenched (*wq*), (ii) furnace cooled (*fc*) or (iii) water quenched and annealed at different temperatures (*wq + an*) for 2h. Information about the studied alloys is collected in Table 1.

## 2.2. Methods

Light microscopy, scanning (SEM) and transmission (TEM) electron and magnetic force (MFM) microscopy, X-ray diffraction (XRD), vibrating sample magnetometry (VSM), heat flow (DSC) and mechanical spectroscopy (MS) were employed in this study. TEM investigations were performed by JEOL

JEM1400 transmission electron microscope operated at 120 kV. The thin foils were prepared by electropolishing at a temperature of –25 °C and applied voltage of 23 V in HClO<sub>4</sub>-ethanol-2-Butoxyethanol (A2) electrolyte using Struers TenuPol 5 double-jet polisher. Thermal analysis was carried out using Lab-sys Setaram equipment with heating rates from 20 to 40 K min<sup>–1</sup>. The magnetic hysteresis loop was measured at room temperature (RT) using vibrating sample magnetometer (Foner magnetometer Oxford). The structure of samples was examined by X-ray diffraction (XRD) analysis using a Bruker D8 Advanced diffractometer with Cu K $\alpha$  radiation.

MS is the simultaneous testing of anelastic (internal friction,  $Q^{-1}$ ) and elastic (Young's modulus,  $E$ ) properties. We measured frequency-, amplitude- and temperature dependent internal friction (IF) and elastic modulus (FDIF, ADIF, TDIF) using forced bending (dynamical mechanical analyzers Q800 TA Instruments and DMA50 Metravib). IF was measured as  $\tan\varphi$  ( $= Q^{-1}$ ) at forced vibrations, where  $\varphi$  is the phase lag between the applied cyclic stress and the resulting strain:  $\sigma = \sigma_0 \cos(\omega t)$  and  $\varepsilon = \varepsilon_0 \cos(\omega t + \varphi)$ ;  $\omega = 2\pi f$  and  $\varphi$  is the phase or loss angle.

## 2.3. Results

FDIF tests were carried out using forced vibrations at DMA (bending,  $f$  from 0.01 to 200 Hz,  $\varepsilon_0 = 0.007\%$ ) and pendulum (torsion, 0.0001–50 Hz,  $\varepsilon_0 = 0.0005\%$  [7]). Figure. 2a shows DMA tests at RT for several alloys and the choice of frequencies for TDIF tests. Tests performed at  $f > 30$ –40 Hz exhibit an artificial peak-like effect due to an unfortunate ratio of sample and apparatus stiffness: absolute damping values in this range are not reliable. An increase of relaxation time with lowering frequency below 30Hz leads to a slight decrease in modulus and increase in damping. The highest reliable damping values in this range

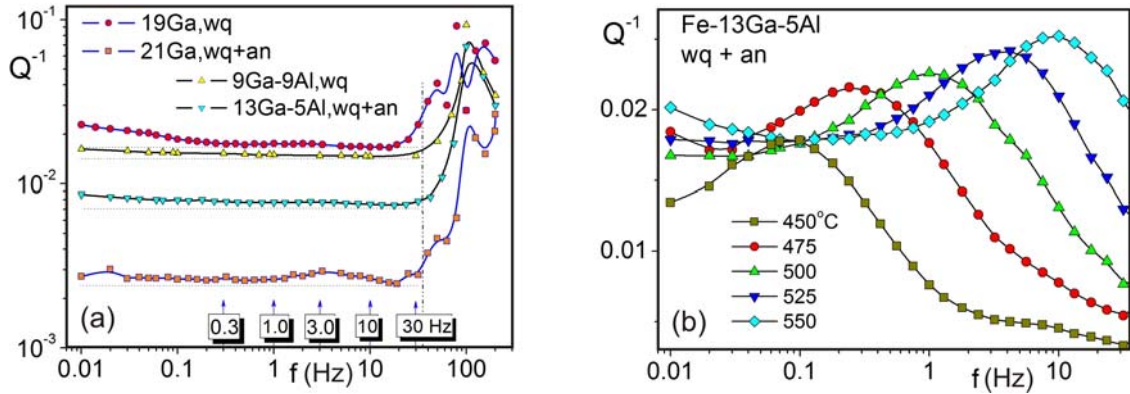


Fig. 2. FDIF tests at (a) RT for several Fe-Ga-(Al) alloys in *wq* and *wq + an* states, (b) 450–550 °C (P3) for Fe-12Ga-5Al *wq + an* sample.

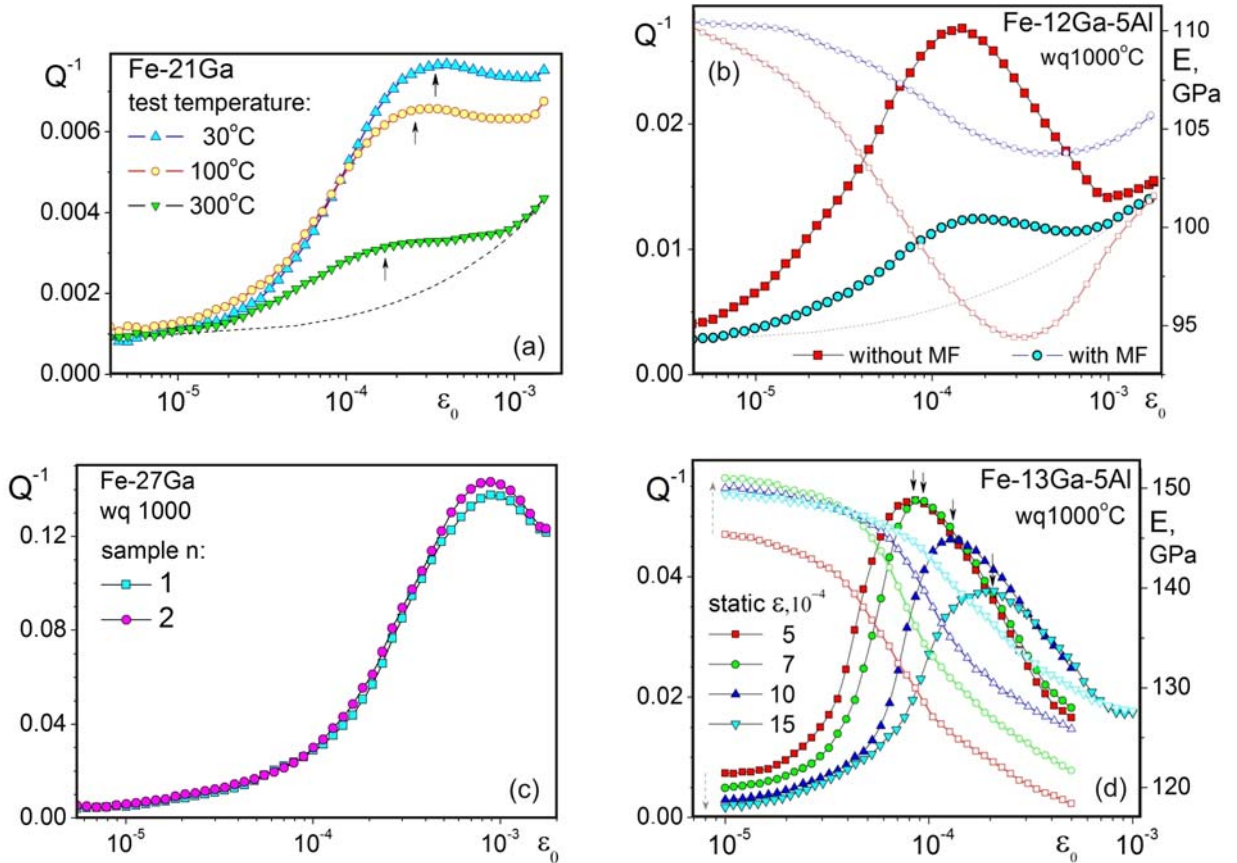


Fig. 3. ADIF tests: (a) at different temperatures, (b) with and without magnetic field, (c) after *wq* and *wq + ann*, (d) different static stress.

correspond to Fe-19Ga, the lowest – to Fe-21Ga alloys. Tests at  $f < 0.3$  Hz are time consuming: for TDIF tests with a typical heating rate of  $1 \text{ K min}^{-1}$  they lead to a low density of experimental points. Thus, five frequencies: 0.3, 1, 3, 10 and 30 Hz were chosen for TDIF and  $f = 3$  Hz for ADIF tests with a fixed temperature. Figure 2b shows the FDIF results at 450–550 °C in the vicinity of the P3 peak (see below).

*ADIF: influence of composition, magnetic field,*

*temperature and scheme of loading.* Most of studied Fe-Ga-based alloys exhibit a peak at ADIF at  $(1-3) \times 10^{-4}$ , the height of which decreases with increase in test temperature (Fig. 3a) and in magnetic field (b) proving its magneto-mechanical origin. The influence of heat treatment is complicated: for alloys with  $< 13$  % Ga furnace cooling leads to highest damping, while residual stresses in quenched state decrease damping. For alloys with about 13–20 % Ga quenching

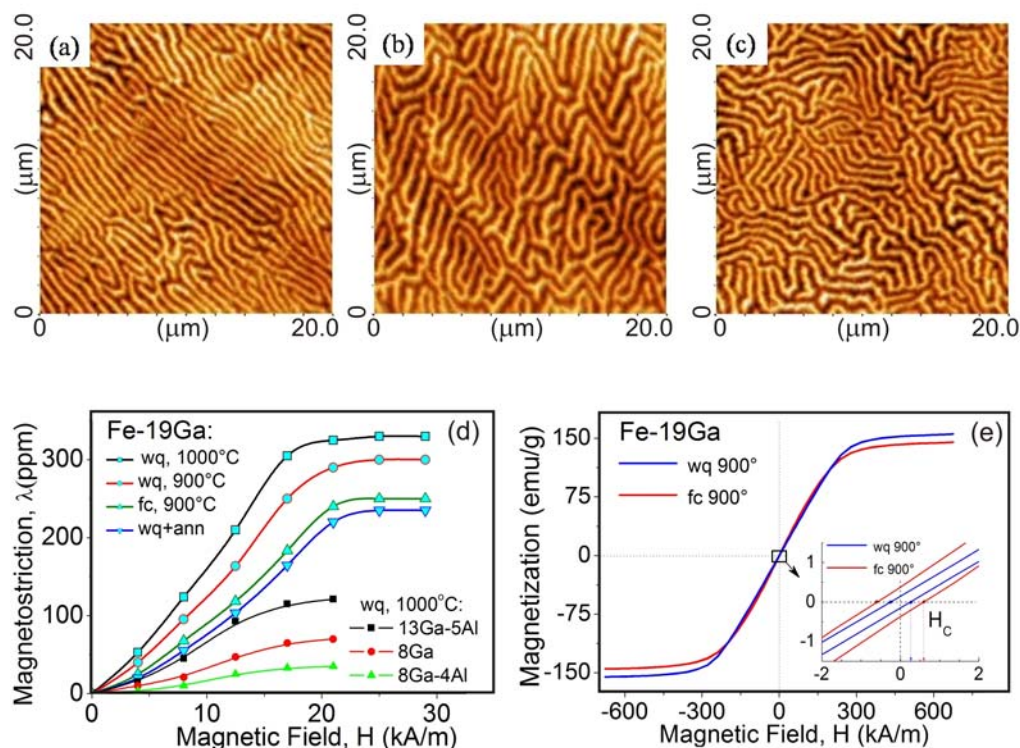


Fig. 4. Magnetic domains in  $wq_{900^\circ}$  (a),  $fc_{900^\circ}$  (b) and  $wq_{an350^\circ}$  (c) Fe-19Ga samples; magnetostriction curves (d) for Fe-19Ga ( $wq_{1000^\circ}$ ,  $wq_{900^\circ}$ ,  $fc_{900^\circ}$ ,  $wq_{an350^\circ}$ ) and  $wq_{1000^\circ}$  Fe-8Ga, Fe-8Ga-4Al and Fe-13Ga-5Al specimens; Magnetization curves (e) for Fe-19Ga ( $wq_{900^\circ}$ ,  $fc_{900^\circ}$ ): inset – data magnification around 0 field.

leads to highest damping; furnace cooling and annealing after quenching decreases damping due to ordering processes in the alloys. In alloys with 21–23 % Ga damping is low even in water quenched state. Damping in Fe-27Ga becomes again much higher (Fig. 3c).

Absolute damping values depend on test conditions. Three point bending tests exhibit higher damping (d) compared with cantilever tests due to different stress distribution in the sample [8]. Increase in static strain from 5 to  $15 \times 10^{-4}$  lowers damping and shifts the peak to higher amplitude. With increase of static stress MDs adjust their shape and volume to applied stress: their mobility under cyclic stress becomes lower and damping decreases. Highest damping at three point bending ( $\tan \varphi \approx 0.05$ ) is recorded for binary (18–19) %Ga alloys. Free decay tests give damping nearly twice higher than forced bending vibrations in cantilever mode. Substitution of Ga by Al atoms decreases damping and magnetostriction (Fig. 4) by 20–25 %.

**Magnetostriction and the structure of magnetic domains.** Magnetic domain patterns of the  $wq$ ,  $fc$ , and  $wq + an$  Fe-19Ga alloy are shown in Fig. 4 a-c, correspondingly. Stripe-like domains with a high degree of alignment dominate due to an increasing perpendicular anisotropy in the  $wq$  sample. Average domain width is  $\approx 0.5 \mu\text{m}$  and its length is above  $10 \mu\text{m}$ . In contrast, irregular maze-like domain patterns with a low degree

of alignment typical for ordered atomic structure are found in the  $fc$  and  $wq + an$  samples.

Magnetostriction curves for several  $wq$  Fe-Ga-based alloys are shown in Fig. 4d, magnetization curves – in Fig. 4e. These figures underline: (i) an increase in  $\lambda_S$  with Ga up to 19 %; (ii) the role of heat treatment: furnace cooling and annealing after quenching provoke atomic ordering, which opposes magnetic DWs motion, decreases saturation magnetostriction  $\lambda_S$  (from 310 to 220 ppm), magnetization  $M_S$  (from 155 to 144  $\text{emu g}^{-1}$ ), and increases coercive force  $H_C$  (from 240 to 560  $\text{A m}^{-1}$ ) and hardness (HV from 250 to 272–281); (iii) a decrease in  $\lambda_S$  with substitution of Ga or Fe by Al.

**Temperature dependent effects.** TDIF original results have been presented in our papers [7, 11–17]. In this paper, we suggest two schemes which describe most of the experimental data (Fig. 5). Both schemes have at least two thermally activated IF peaks P1 and P3, they also have a range of irreversible structural transition (ST) at 150–300°C, characterized by an increase in the modulus. The main difference occurs in the range of 300–450°C. The P2 peak in scheme (a) is at least partly a thermally activated effect, in contrast the  $P_{Tr}$  peak temperature in scheme (b) does not depend on testing frequency. The relaxation strength of both peaks rapidly decreases with increase in frequency.

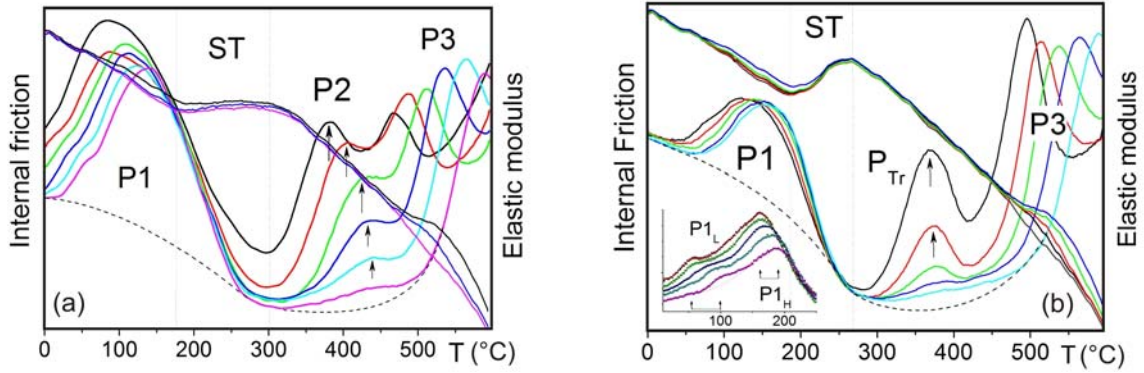


Fig. 5. Typical schemes for TDIF at heating of quenched Fe-Ga alloys.

Table 2. Anelastic effects in selected Fe-Ga-based alloys after water quenching from 1000 °C

Effect	Alloy	$H$ (eV)		$\tau_0$ (s)		Ref.
		Heating	(Cooling)	Heating	(Cooling)	
P1 <sub>L</sub>	Fe-8Ga	0.95 ± 0.06		$4 \times 10^{-15}$		
	Fe-13Ga	0.88–0.93		$8 \times 10^{-15}$ – $2 \times 10^{-16}$		[14]
	Fe-18Ga	0.79 ± 0.43		$2 \times 10^{-13}$		[16]
	Fe-21Ga	0.72 ± 0.33		$3 \times 10^{-12}$		[16]
	Fe-8Al-3Ga	0.82 ± 0.03		$5 \times 10^{-14}$		[11]
	Fe-18Ga-5Al	1.12 ± 0.04		$4 \times 10^{-16}$		[17]
P1 <sub>H</sub>	Fe-8Ga	1.29 ± 0.13		$1 \times 10^{-18}$		this work
	Fe-13Ga	1.04–1.16		$6 \times 10^{-14}$ – $4 \times 10^{-17}$		[7]
	Fe-21Ga	1.22 ± 0.33		$2 \times 10^{-18}$		[16]
	Fe-23Ga	1.21 ± 0.07		$6 \times 10^{-18}$		this work
	Fe-27Ga	1.05 ± 0.01		$9 \times 10^{-15}$		this work
	Fe-8Al-3Ga	1.07 ± 0.04		$4 \times 10^{-16}$		[11]
	Fe-18Ga-5Al	1.41 ± 0.04		$2 \times 10^{-18}$		[17]
P2	Fe-13Ga	2.43 ± 0.05		$1 \times 10^{-17}$		[7, 13]
	Fe-17Ga	2.12		$6 \times 10^{-17}$		[14]
	Fe-20Ga	2.29–2.68 (2.44–2.65)		$10^{-17}$ – $10^{-18}$ ( $10^{-18}$ – $10^{-19}$ )		[12]
P3	Fe-8Ga	3.19 ± 0.09		$2 \times 10^{-20}$		this work
		2.70		$2 \times 10^{-16}$		[7, 11]
	Fe-13Ga	2.53 ± 0.05 (2.48 ± 0.07)		$8 \times 10^{-18}$ ( $1 \times 10^{-17}$ )		[13]
		2.86		$3 \times 10^{-20}$		[12]
	Fe-17Ga	2.48 ± 0.10		$5 \times 10^{-18}$		[11]
	Fe-18Ga	2.87 ± 0.08 (2.71 ± 0.09)		$6 \times 10^{-21}$ ( $6 \times 10^{-20}$ )		[15, 16]
	Fe-21Ga	2.84 ± 0.03 (2.69 ± 0.09)		$8 \times 10^{-21}$ ( $6 \times 10^{-20}$ )		[16]
	Fe-23Ga	2.47 ± 0.11		$7 \times 10^{-18}$		this work
	Fe-8Al-3Ga	2.71/2.68		$1 \times 10^{-18}$		[11]
Fe-13Al-5Ga	2.8		$1 \times 10^{-18}$		[11]	

The P1 peak (Fig. 5) represents a broad relaxation effect. It can be reliably decomposed into two components in several tests: P1<sub>L</sub> and P1<sub>H</sub> (inset to Fig. 5b). According to activation parameters these peaks (Table 2) were interpreted as the Snoek type peaks with two components Fe-C-Fe and Fe-C-(Ga,Al) for alloys containing up to 13 % Ga [7, 11]. Addition of strong carbide forming Nb

eliminates these peaks and annealing leads to decrease of IF nearly to the background level shown by the dotted line. In high Ga containing alloys (> 18 % Ga) one can also distinguish the P1<sub>L</sub> and P1<sub>H</sub> peaks, however a structural transition, which starts above 150 °C, suppresses thermally activated relaxation processes and sometimes does not allow reliable calculations of activation parameters. The

double headed P1 peak is well recorded in Fe-18Ga-5Al alloy [17].

*Structural transition, ST*, at 150–300°C (Fig. 5) is accompanied by relative increase in modulus and contraction at dilatometry tests, an exothermal peak at heat flow, and increase in hardness [11, 15, 16]. From the dependence of ‘a peak at heat flow curves vs heating rate’ the activation energy of the corresponding process estimated by Kissinger method is in the range from 0.95 eV for binary alloys with 8–13 % Ga to 0.5 eV for alloys with 18–22 % Ga and ternary 18 % (Ga + Al) alloys.

After water quenching the structure of samples with 19–27 % Ga is A2 (dominating phase) and D0<sub>3</sub>. Overlapping of XRD reflections from planes (310) A2 and (620) D0<sub>3</sub> at around 2θ 113–114° takes place. According to positron annihilation spectroscopy [16] and XRD [17] studies the main processes in the temperature range of structural transition at 150–300°C are decrease in vacancy concentration and D0<sub>3</sub> ordering. Ordering up to 300°C leads to a shift of the main intensity of XRD reflection around 113° to higher angles, i.e. to D0<sub>3</sub> structure. Annealing at 400 and 500°C leads to nucleation and growth of L1<sub>2</sub> phase (Fig. 6a). Corresponding microstructure after annealing at 400°C during five hours is shown in Fig. 6d.

Above the ST alloys with relatively low Ga % behave according to scheme (a), i.e. they have a combination of P2 and P3 peaks (Fig. 5). The Fe-17%Ga-NbC alloys belong to this group, too. For alloys with higher Ga content and/or additions of Al the scheme (b) is more typical. Activation parameters of the P2 and P3 peaks calculated using both TDIF and FDIF tests are given in Table 2.

*The P2 peak* (Fig. 5) temperature increases with saturation due to increase in the test frequency and its height decreases rapidly. Increase in annealing temperature (from 730 to 1100°C in Fe-17Ga or from 800 to 900°C in Fe-13Ga) before quenching increases the P2 peak height. The FDIF tests of this peak in Fe-13Ga gave following values for constant temperature:  $H = 0.85$  eV and  $\tau_0 = 10^{-6}$  [7], which are very different from TDIF results at instant heating rate (2.4 eV and  $\tau_0 = 10^{-17}$  [14]), and leave the interpretation of the physical mechanism of this effect open. The frequency independent P<sub>Tr</sub> peak appears in alloys with higher Ga content and it may influence the P2 peak parameters.

*The P<sub>Tr</sub> peak height* (Fig. 5) is irreversibly proportional to measuring frequency:  $Q_{Tr}^{-1} = A \times f^{-1}$ , this dependence is known for transient effects in displacive transformations. In [13] we proposed that this peak is due to the D0<sub>3</sub> → L1<sub>2</sub> transition. Indeed, the formation of short-range D0<sub>3</sub> ordered domains at the first stage of annealing (according to XRD data – Fig. 6a) or even after quenching (TEM image of D0<sub>3</sub> domains – Fig. 6b) is followed by the D0<sub>3</sub> → L1<sub>2</sub> transition at the

second stage (Fig. 6a – XRD and Fig. 6d – SEM). Even this transition is diffusion controlled, elements of a displacive shear transformation are involved due to loss of stability or buckling {110}<110> of the D0<sub>3</sub> phase with formation of metastable closed packed structure [18–20]. The Bain strain is required for the diffusionless part of cubic to tetragonal displacive transformation that brings the structure closer to an equilibrium fcc-based L1<sub>2</sub> ordered phase. The features of the P<sub>Tr</sub> peak are typical for shear transformations and, thus, it can be associated only with D0<sub>3</sub> → L1<sub>2</sub> transformation in studied alloys which is well proved by XRD data (Fig. 6a). Huge P<sub>Tr</sub> peak is recorded in Fe-27Ga alloy (Fig. 6c) which structure below 620°C consists of 100 % L1<sub>2</sub> phase according to the equilibrium diagram. The L1<sub>2</sub> phase appears rapidly in Fe-27Ga alloy above 400°C and is identified by XRD, SEM and TEM. Sequence of phase transitions A2 → D0<sub>3</sub> (metastable ordered phase) → L1<sub>2</sub> (stable ordered phase) is in agreement with experimental data on temperature dependences of  $Q^{-1}$ ,  $E$ , heat flow, dilatometry, positron lifetime and hardness.

*The P3 peak* is observed in all alloys, except of Fe-27Ga, at heating, cooling and in subsequent heating-cooling tests, as well as at FDIF tests (Fig. 2b). Activation energy of this peak varies from 2.5 to 3.2 eV and typical values for  $\tau_0$  range from  $10^{-18}$  to  $10^{-20}$  s. These activation parameters correspond to Zener relaxation in Fe-based alloys [21]. The peak height is smaller in the first heating test and it increases at cooling, remaining practically unchanged in the following tests.

*At cooling* after heating to 600°C only the P3 peak is recorded in most alloys and it is slightly higher than at heating (Fig. 7): this is typical for Zener relaxation in alloys with atomic ordering [22]. Decrease in grain size increases the P3 peak relaxation strength and enhances high temperature IF background, while the presence of NbC particles increases the activation energy of the P3 peak [12] giving some arguments in favour of grain boundary sliding origin of the P3 peak. Heating of *wq* samples to temperatures below 600°C (e.g. 400°C) decreases the P1 peak, mainly its P1<sub>H</sub> component, giving additional opportunities to calculate the P1<sub>L</sub> activation parameters. IF background at cooling increases below the P3 peak with decrease in temperature, which is typical for materials with magnetomechanical damping (Fig. 7). There are some variations: curves of type (1) are recorded in 18Ga, 12Ga-5Al, 9Ga-8Al, 5Ga-12Al alloys, (2) in 8Ga-4Al, 13Ga-5Al, and (3) in 8, 13, 17, 19, 21, 23Ga and 8Al-3Ga. Sometimes the difference between types 1 and 3, 1 and 2 is very small. These variations are due to the competition between two opposite effects: increase of magnetomechanical damping in ferromagnetic phases, mainly in the A2 phase, with lowering temperature, and decrease of damping by nonmagnetic particles of

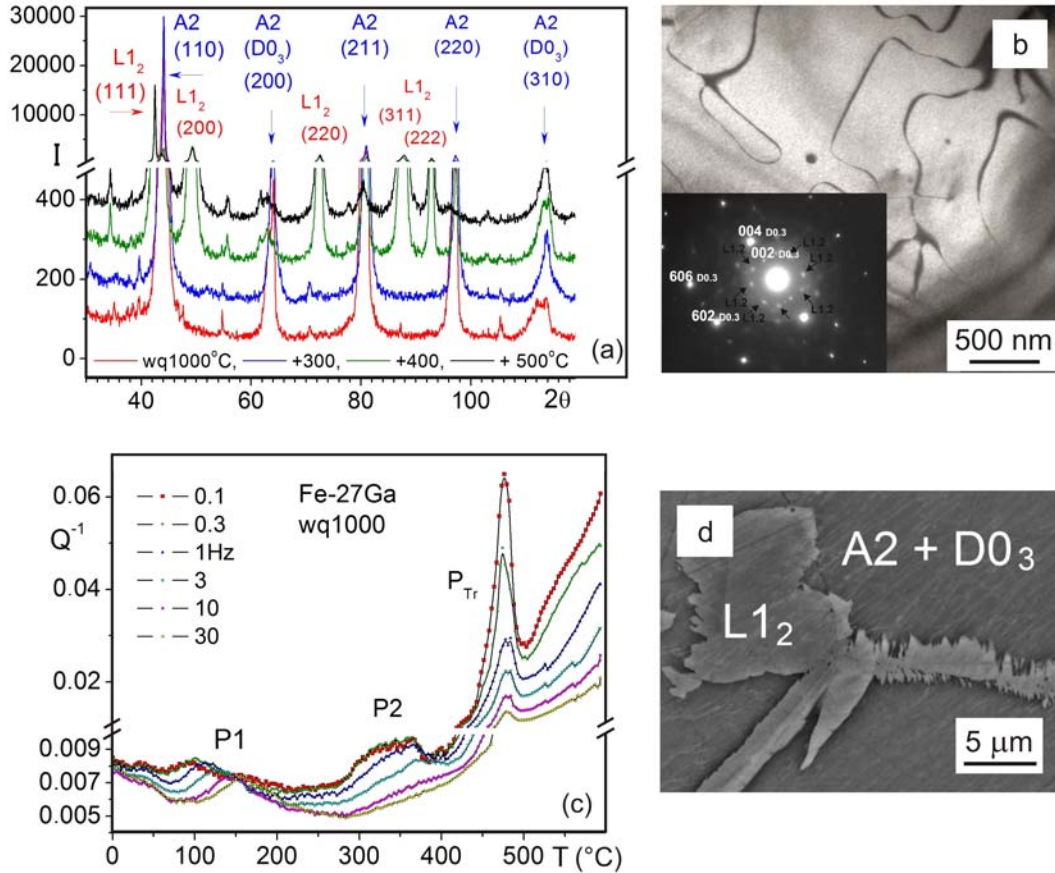


Fig. 6. Fe-27Ga: (a) XRD for water quenched and annealed states, (b) TEM picture after water quenching from 1000 °C (bright field image taken in 002 D0<sub>3</sub> reflection and corresponding diffraction pattern (inset) with zone axis [010] D0<sub>3</sub>. Black arrows mark weak reflections from L1<sub>2</sub> phase), (c) TDIF for water quenched sample, (d) SEM microstructure after annealing at 400 °C, 5 h.

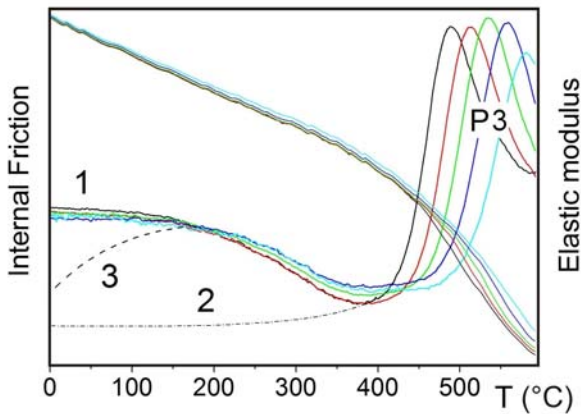


Fig. 7. Scheme for TDIF at cooling.

the L1<sub>2</sub> phase and the D0<sub>3</sub> ordering which did not reach their equilibrium during first heating to 600 °C.

### 3. Summary

In this paper we continue our study of hysteretic

and relaxation damping mechanisms in steels and iron based alloys published earlier in Kovove Mater. [23, 24]. FDIF, ADIF and TDIF spectrometry of Fe-Ga based alloys with high magnetostriction was carried out. Fe-Ga alloys exhibit rather high damping capacity which increases with increase in Ga content up to ~ 19 at.% ( $\Psi \approx 2\pi Q^{-1}$  up to 30 % at forced bending vibrations), then it becomes lower at Ga > 20 %, and again reaches maximum at Ga content 27 at.%. The main contribution to damping comes from magnetomechanical coupling: the D0<sub>3</sub> and L1<sub>2</sub> ordering suppresses damping. The lower limit at which short range D0<sub>3</sub> ordering in Fe-Ga alloys may take place is lower than that shown in Fig. 1. This conclusion is in agreement with the results of the transmission synchrotron X-ray study [25], where short range B2 ordering was reported.

In most cases there is a correlation between magnetostriction values, magnetic structure and damping capacity. The absolute values of damping depend on the test method: forced vibration tests give lower damping compared to free decay tests, cantilever clamping decreases damping compared to three point bending tests, static stress also decreases damping and

shifts maximum to higher amplitude of vibrations.

Substitution of Ga by Al atoms smoothly decreases damping capacity of Fe-Ga alloys. Aluminium stabilizes the D0<sub>3</sub> ordered phase. D0<sub>3</sub> ordering precedes the appearance of the equilibrium L1<sub>2</sub> phase, the D0<sub>3</sub> → L1<sub>2</sub> transition causes the  $P_{Tr}$  peak at TDIF curves at heating. Broad P1 peak represents several relaxation effects caused mainly by point defects, and it is affected by the first step of the ordering reaction: A2 → D0<sub>3</sub>. The P3 peak is probably due to Zener relaxation. The P2 effect is a combination of thermally activated relaxation effect and effect of the L1<sub>2</sub> phase nucleation in the alloys.

### Acknowledgements

This paper is set for the Prof. Pavel Lukáč's special edition.

The authors gratefully acknowledge the financial support of the RFBR (Russia) research project 14-03-00165a, the Ministry of Education and Science of the Russian Federation in the frameworks of Increase Competitiveness Program of MISIS and State Task for Universities (1855).

### References

- [1] Clark, A. E., Hathaway, K. B., Wun-Fogle, M., Restorff, J. B., Lograsso, T. A., Keppens, V. M., Petculescu, G., Taylor, R. A.: *J. Appl. Phys.*, **93**, 2003, p. 8621. [doi:10.1063/1.1540130](https://doi.org/10.1063/1.1540130)
- [2] Srisukhumbowornchai, N., Guruswamy, S.: *J. Appl. Phys.*, **90**, 2001, p. 5680. [doi:10.1063/1.1412840](https://doi.org/10.1063/1.1412840)
- [3] Ishimoto, M., Numakura, H., Wuttig, M.: *MSE (A)*, **442**, 2006, p. 195. [doi:10.1016/j.msea.2006.02.215](https://doi.org/10.1016/j.msea.2006.02.215)
- [4] Smith, G. W., Birchak, J. R.: *J. Appl. Phys.*, **39**, 1968, p. 2311. [doi: 10.1063/1.1656551](https://doi.org/10.1063/1.1656551)
- [5] Ruffoni, M. P., Pascarelli, S., Grossinger, R., Turtelli, R. S., Bormio-Nunes, C., Pettifer, R. F.: *Phys. Rev. Lett.*, **101**, 2008, p. 147202. [doi:10.1103/PhysRevLett.101.147202](https://doi.org/10.1103/PhysRevLett.101.147202)
- [6] Ikeda, O., Kainuma, R., Ohinuma, I., Fukamichi, K., Ishida, K.: *JALCOM*, **347**, 2002, p. 198. [doi:10.1016/S0925-8388\(02\)00791-0](https://doi.org/10.1016/S0925-8388(02)00791-0)
- [7] Golovin, I. S., Rivière, A.: *Intermetallics*, **19**, 2011, p. 453. [doi:10.1016/j.intermet.2010.10.017](https://doi.org/10.1016/j.intermet.2010.10.017)
- [8] Xiaofeng, H., Shuwei, L., Xiuyan, L., Lijian, R.: *Chinese J. Mat. Research*, **27**, 2013, p. 225. [doi:10.1005-3093\(2013\)03-0225-06](https://doi.org/10.1005-3093(2013)03-0225-06)
- [9] Bai, F., Zhang, H., Li, J., Viehland, D.: *Applied Physics Letters*, **95**, 2009, p. 152511. [doi: 10.1063/1.3238062](https://doi.org/10.1063/1.3238062)
- [10] Emdadi, A. A., Cifre, J., Dementeva, O. Yu., Golovin, I. S.: *JALCOM*, **619**, 2015, p. 58. [doi: 10.1016/j.jallcom.2014.08.231](https://doi.org/10.1016/j.jallcom.2014.08.231)
- [11] Golovin, I. S., Belamri, Z., Hamana, D.: *JALCOM*, **509**, 2011, p. 8165. [doi: 10.1016/j.jallcom.2011.04.138](https://doi.org/10.1016/j.jallcom.2011.04.138)
- [12] Fang, M., Zhu, J., Golovin, I. S., Li, J., Yuan, Ch., Gao, X.: *Intermetallics*, **29**, 2012, p. 133. [doi:10.1016/j.intermet.2012.05.015](https://doi.org/10.1016/j.intermet.2012.05.015)
- [13] Golovin, I. S.: *The Physics of Metals and Metallography*, **114**, 2013, p. 1018. [doi:10.1134/S0031918X13090056](https://doi.org/10.1134/S0031918X13090056)
- [14] Golovin, I. S., Cifre, J.: *JALCOM*, **584**, 2014, p. 322. [doi: 10.1016/j.jallcom.2013.09.077](https://doi.org/10.1016/j.jallcom.2013.09.077)
- [15] Golovin, I. S., Palacheva, V. V., Zadorozhnyy, V. Yu., Zhu, J., Jiang, H., Cifre, J., Lograsso, T. A.: *Acta Materialia*, **78**, 2014, p. 93. [doi:10.1016/j.actamat.2014.05.044](https://doi.org/10.1016/j.actamat.2014.05.044)
- [16] Golovin, I. S., Dubov, L. Yu., Funtikov, Yu. V., Palacheva, V. V., Cifre, J., Hamana, D.: *Met. Mat. Trans. A*, **46**, 2015, p. 1131. [doi:10.1007/s11661-014-2721-3](https://doi.org/10.1007/s11661-014-2721-3)
- [17] Golovin, I. S., Palacheva, V. V., Bazlov, A. I., Cifre, J., Pons, J.: *JALCOM*, accepted. [doi:10.1016/j.jallcom.2015.04.150](https://doi.org/10.1016/j.jallcom.2015.04.150)
- [18] Boisse, J., Zapolsky, H., Khachatryan, A. G.: *Acta Mat.*, **59**, 2011, p. 2656. [doi: 10.1016/j.actamat.2011.01.002](https://doi.org/10.1016/j.actamat.2011.01.002)
- [19] Khachatryan, A. G., Viehland, D. D.: *Metal. Mater. Trans. A*, **38**, 2007, p. 2317. [doi:10.1007/s11661-007-9253-z](https://doi.org/10.1007/s11661-007-9253-z)  
<http://www.vupp.cz/czvupp/04bezlepkove/>
- [20] Khachatryan, A. G., Viehland, D. D.: *Metal. Mater. Trans. A*, **38**, 2007, p. 2308. [doi: 10.1007/s11661-007-9252-0](https://doi.org/10.1007/s11661-007-9252-0)
- [21] Blanter, M. S., Golovin, I. S., Neuhäuser, H., Sinning, H.-R.: *Internal Friction in Metallic Materials. A Handbook*. Berlin, Springer Verlag 2007.
- [22] Golovin, I. S., A. Rivière, A.: *Intermetallics*, **14**, 2006, p. 570. [doi:10.1016/j.intermet.2005.09.010](https://doi.org/10.1016/j.intermet.2005.09.010)
- [23] Puškar, A., Golovin S.: *Kovove Mater.*, **16**, 1978, p. 426.
- [24] Golovin, S., Puškar, A., Golovin, I.: *Kovove Mater.*, **21**, 1983, p. 305.
- [25] Du, Y., Huang, M., Chang, S., Schlagel, D. L., Lograsso, T. A., McQueeney, R. J.: *Physical Review B*, **81**, 2010, p. 054432. [doi:10.1103/PhysRevB.81.054432](https://doi.org/10.1103/PhysRevB.81.054432)